Photo-generation of cyclic carbonates using hyper-branched Ru-TiO_2

Journal Name

ARTICLE

Photo-generation of Cyclic Carbonates Using Hyper-branched Ru-TiO_2

Received 00th January 20xx,
Accepted 00th January 20xx

DOI: 10.1039/x0xx00000x

www.rsc.org/

Stelios Gavrielides [a], Jeannie Z. Y. Tan [a], Eva Sanchez Fernandez[a] and M. Mercedes Maroto–Valer*[a]

Anthropogenic CO_2 is the main contributor to the increased concentration of greenhouse gases in the atmosphere, and thus utilising waste CO_2 for the production of valuable chemicals is a very appealing strategy for reducing CO_2 emisions. The catalytic fixation of CO_2 with epoxides for the production of cyclic carbonates has gained increasing attention from the research community in search of an alternative to the homogeneous catalytic routes, which are currently being used in industry. A novel photocatalytic heterogeneous approach to generate cyclic carbonates is demonstrated in this work. Hyper-branched microstructured Ru modified TiO_2 nanorods decorated with RuO_2 nanoparticles, supported on fluorine-doped tin oxide (FTO) glass were fabricated for the first time and were used to catalyse the photo-generation of propylene carbonates from propylene oxides. Propylene carbonate was used as a reference for cyclic carbonates. The photo-generation of cyclic carbonates from epoxides and CO_2 was carried out at a the maximum temperature of 55 °C and 200 kPa in a stainless steel photoreactor with a quartz window, under solar irradiation. The best performing photocatalyst exhibited an estimated selectivity of 83% towards propylene carbonates under the irradiation of solar simulator.

Introduction

Humankind relies heavily on fossil fuels as the primary energy source, producing CO_2 as a by-product, which is released into the atmosphere. The increased level of anthropogenic CO_2 emissions is one of the most vital contributors to climate change. In this regards, the research community has been trying to address this challenge by developing alternative energy sources, increasing efficiency and carbon capture, utilisation and storage (CCUS).[1] Utilising CO_2 in the production of commercially valuable chemicals and fuels has recently attracted much attention.[2] CO_2, is often a good source of C-building blocks for various organic synthesis, as it is abundant and low-cost.[3] Using waste CO_2 as a feedstock for chemical reactions not only offers a more sustainable route to generate value-added products, but also contributes to CO_2 fixation.[1,4]

The synthesis of cyclic carbonates (CCs) through the coupling of CO_2 and epoxides has been commercially available for over 60 years and is one of the most promising CO_2 utilisation industrial applications.[1] CCs are valuable as monomers, small molecules[5] and polymer intermediates,[6] pharmaceuticals[7], and fine chemical intermediates.[3] In addition, the most important and rapidly growing application of CCs lies in Li-ion batteries, in which CCs are used as electrolytes.[8] Nowadays, Li-ion batteries power most of the portable electronic devices and their application in electronic vehicles is becoming very popular.[8] Due to the future projected demands for Li-ion batteries, the current industrial production of Li-ion is rapidly increasing.

Current commercial process for CCs synthesis uses homogeneous catalysts, such as quaternary ammonium[9] or phosphonium halides. Although these catalysts are inexpensive, they suffer from low efficiencies and require high temperature and pressure.[10] More specifically, the reaction conditions were reported to be at 100-200 °C, and 50-100 bar.[11] Additionally, due to their corrosive nature, special reactor materials are necessary, which further increases the production cost. Hence, in recent decades, new approaches have been developed for the production of CCs.[12-15] Many researchers used homogeneous catalysts, such as (salen)Cr(III) complexes[3], (salen)Co(III),[16] (salen)Mn(III),[17] and supramolecular metal complexes[18] to catalyse the production of CCs. However, several drawbacks were detected have been reported for these developed homogeneous catalysts, including low catalyst stability, reactivity and air sensitivity.[3,8] Furthermore, the recovery of these homogeneous catalysts, and the purification of the product is challenging, expensive and time-consuming.[1]

Recently, heterogeneous catalysts for the synthesis of CCs have been developed because of the easy separation of fluids from the solid catalyst, convenient handling and catalyst regeneration.[1,19] For example, Zn-ZIF-67-MOFs,[20] Fe(III)[21] and bimetallic complexes[22] have been developed to catalyse the production of CCs from CO_2 and epoxide.

Photocatalysis has received much attention from the research community in the recent years due to its sustainability aspect and its high performance in a variety of applications, including photo-generation of H_2,[23-26] photoreduction of CO_2 for the production of fine chemicals and solar fuels,[27-29] and air and water purification.[30-32] TiO_2 is the most widely used photo-

[a] Research Centre of Carbon Solutions (RCCS), School of Engineering & Physical Sciences, Heriot–Watt University, Edinburgh, United Kingdom.
*Corresponding author: M.Maroto-Valer@hw.ac.uk Address here.

catalyst for these applications because it is non-toxic, thermally and chemically very stable, abundantly available and has good photo-response under UV light irradiation.[33,34]

Very recently, Prajapati *et al*. demonstrated the first photocatalytic synthesis of CCs using cobalt phtalocyanine grafted on TiO_2, The synthesized photocatalyst revealed 94.2% of conversion after 24 h of irradiation at 25 °C and 1 atm. Additionally, the photocatalysis route has shown promising performance and provides a safer route with milder reaction conditions, compared to other heterogeneous catalysts, which were reported to require temperatures up to 80-150 °C and pressure of 10 - 30 bar.[19]

To further explore the photogeneration of CCs using TiO_2-based heterogeneous photocatalysts, the use of a thin film photocatalyst is proposed here to eliminate the need of separation step to recycle the catalyst, as well as to ease the handling of photocatalyst. To the best of the authors' knowledge, the photo-generation of CCs using a thin film photocatalyst has not been reported in the literature. TiO_2 is a wide band gap semiconductor, and thus, it is photo-active predominantly in the UV range. To address this issue, the addition of foreign elements that are active in the visible light region are employed. RuO_2 decorating the TiO_2 are known to increase the overall absorbance of the RuO_2/TiO_2 material in the visible light region.[35] Therefore, the combination of Ru^{4+} doping and RuO_2 decoration on the TiO_2 can greatly increase the absorbance in the visible light region, and in turn making the use of solar light viable.[36] Furthermore, RuO_2 has high chemical stability, and electrical conductivity. The combination of RuO_2 with TiO_2 has been reported to improve charge separation, hindering the recombination process which should enhance the photocatalytic activity of the material.[35] This effect is attributed to the position of RuO_2 valence and conduction band relative to those of TiO_2. Therefore, in this work, Ru_x-TiO_2 thin film supported on the fluorine-doped tin oxide (FTO) glass is proposed for photogeneration of CCs.

Moreover, in order to provide large surface area with more exposed active sites and superior light scattering capability, fast electron transport and efficient charge collection, the hyper-branched nanorods (HBN), are synthesized. These HBN have been reported to exhibit improved optical and photoelectrical properties which resulted in improved photo-conversion reactions.[37] Hence, the HBN were modified with Ru to be used as a novel Ru_x-TiO_2 photocatalyst for the photogeneration of CCs.

Experimental

Materials

Fluorine-doped tin oxide (FTO) glass TEC-15 was purchased from Ossila (dimensions 2.5 cm x 2.5 cm, roughness of 12.5 nm, FTO layer thickness of 200 nm, 83.5% transmission and resistivity of 12-14 $\Omega.cm^{-1}$). Potassium titanium oxide oxalate dihydrate (PTO, ≥98.0%), diethylene glycol (DEG, 99.0%), bis(cyclopentadienyl)ruthenium ($(C_5H_5)_2Ru$, 98.0%), *n*-hexane (C_6H_{14}, 95.0%), propylene oxide (PO, 99.0%), dichloromethane (DCM, CH_2Cl_2, 99.8%), 4-(dimethylamino)pyridine (DMAP, 99.0%), propylene carbonate (PC, 99.7% anhydrous) and polyethylene glove Atmosbag were purchased from Sigma-Aldrich. Isopropanol (IPA, 99.5%), acetone (>95.0%) and ethanol (99.0%) were procured from Fisher Scientific. All chemicals were used without any further purification. All aqueous solutions were prepared using Milli-Q ultrapure type 1 water (18.2 MΩ.cm) collected from a Millipore system.

Synthesis

The FTO glass was cleaned prior to use with a solution of H_2O, IPA, and Acetone in a ratio of 1:1:1, for 1 h in the sonicator and air dried at 75 °C for 30 mins.

Hyper-branched nanorods (HBNs) of TiO_2 were fabricated using a hydrothermal approach. PTO was dissolved in a mixture of H_2O and DEG with a ratio of 1:7. The concentration of PTO was 0.05 M. After 30 minutes of vigorous stirring, the precursor solution was transferred to a 100 mL Teflon-lined autoclave along with the FTO glass. The FTO glass was positioned resting against the Teflon-liner walls with the conductive side facing down at approximately 60°. The hydrothermal synthesis was carried out at 180 °C for 9 h. After completing the reaction time, the autoclave was allowed to cool down to room temperature. The TiO_2 nanorods were rinsed several times with Milli-Q Type 1 water and ethanol, and then calcined at atmospheric conditions at 550 °C for 1 h.

The Ru loaded TiO_2 (Ru_x-TiO_2) was synthesized under dry nitrogen atmosphere, in a polyethylene Atmos glovebag. A known amount of bis(cyclopentadienyl)ruthenium $(C_5H_5)_2Ru$, was dissolved in *n*-hexane (C_6H_{14}) and stirred vigorously at 40 °C until a clear solution was obtained. Three different concentrations of Ru precursor were synthesised, namely 0.05 M, 0.01 M, and 0.005 M that are denoted as Ru_{05}-TiO_2, Ru_{01}-TiO_2, and Ru_{005}-TiO_2, respectively. The TiO_2 loaded FTO glass was heated to 150 °C for 1 h to remove adsorbed water and was then allowed to cool to room temperature in dry air. The TiO_2 loaded FTO glass was then placed into the teflon liner resting against its walls at roughly 60 ° with the coated surface facing down. The ruthenium precursor liquid was added to the Teflon-liner to cover the entire FTO surface (25 ml). The Teflon liner was then transferred into the autoclave and was placed in the oven at 180 °C for 30 h. The Ru_x-TiO_2 FTO glass was then rinsed with *n*-hexane in dry nitrogen. It was then calcined to 400 °C for 10 h under dry air atmosphere with a ramp rate of 10 °C min^{-1}.

Characterisation

The morphology of the synthesized products was examined by a field emission scanning electron microscope (FE-SEM, FEI Quanta 200 F). Further investigation on the morphology and the element composition of the samples was carried out using a transmission electron microscope (TEM) and high resolution HR-TEM (FEI Titan Themis 200) equipped with an energy dispersive X-ray spectroscope (EDX) detector operated at 200 kV. The samples were sonicated in ethanol for 5 min and then a few drops of the solution were placed on a carbon-coated copper TEM grid. Crystallinity and

phase identification of the synthesized products were performed using powder X-ray diffraction (XRD, Bruker D8 Advanced Diffractometer) equipped with Cu Kα radiation (λ= 1.5418 Å). Raman spectra were collected using a Renishaw *inVia* Raman Microscope with 785 nm excitation source. The diffuse reflectance was measured using a Perkin Elmer Lambda 950 UV-vis equipped with an integrating sphere (150 mm) and the band gap energy was estimated using the Kubelka Munk function. X-ray photoelectron spectroscopy (XPS) was performed on a Scienta 300 XPS machine incorporating with a rotating AlKα X-ray source operating at 13 kV x 333 mA (4.33 kW). Electron analysis was performed using a 300 cm radius hemispherical analyser and lens system. The electron counting system consist of a multichannel plate, phosphorescent screen and CCD camera. All multichannel detection counting is done using proprietary Scienta software. The elements present were determined *via* a wide energy range survey scan (200 mW step, 20 ms dwell time, 150 eV pass energy and summed over 3 scans). The high resolution scans were performed at a similar pass energy (150 eV), but a step size of 20 mV. A dwell time of 533 ms was used and accumulated over 3 scans. The instrument operated at a base pressure of 1 x 10^{-9} mbar; the energy scale is calibrated using the Au 4f, Ag 3d and Cu 2p emission lines, where the half width of the Au $4f_7$ emission line is approximately 1.0 eV. All data analysis and peak fitting were performed using the CaseXPS software.

Photocatalysis

The reaction solution was prepared with DCM and PO in a 1:8 ratio, adding 1.022 mg of DMAP per mL of solution, and was kept in the dark at room temperature. The solution was then transferred to the stainless steel Teflon-lined pressurized photo-reactor (Scheme 1) along with the photocatalyst. Two control experiments were performed, one with the absence of photocatalyst and light, and one with the absence of light, keeping all the rest reaction conditions the same. The temperature throughout the experiment was measured using a pyrometer from the outside of the reactor that ranged between 40-55 °C. For the experiments incorporating photocatalysts, four pieces of Ru_x-TiO_2 coated FTO glasses were supported on a custom-made photocatalyst stage, as shown in Scheme 1. The stage was positioned directly below the quartz glass to be irradiated with the AM1.5G solar simulator directly (1 sun equivalent, 100 Wm^{-2}, 92250 A Newport, USA) while being submerged in the reaction solution. The reaction solution was bubbled with CO_2 and pressurised in CO_2 atmosphere, throughout the experiment. The 500 mL photo-reactor was supplied with continuous CO_2 and the pressure was maintained at 200 kPa using a bubbler. The reaction was conducted under the solar simulator for 6 h. After the reaction time was completed, the unreacted substrate and solvent were removed *in vacuo* and the products were then isolated using a rotary evaporator. The products were then identified using a FTIR spectrometer Perkin Elmer Frontier.

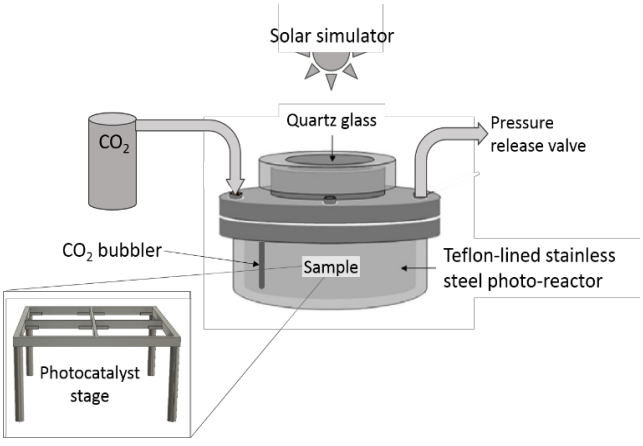

Scheme 1. Schematic diagram of the photocatalysis setup and photocatalytic stage.

Results and discussion

The as-prepared TiO_2 and the fabricated Ru_x-TiO_2 thin film samples synthesized using solvothermal treatment followed by calcination exhibited homogeneous coating on the FTO glass. All the prepared samples were examined using XRD. In addition to the XRD pattern of the FTO coating on the glass, the crystallinity of anatase TiO_2 was also observed in all the samples (Figure 1). The peaks positioned at 25.4 and 48.1° were assigned to the (101) and (200) planes of anatase. No ruthenium related peak was observed in the XRD patterns of the fabricated Ru_x-TiO_2 samples. This was probably due to the low concentration of Ru deposited on the glass. However, it is observed that with higher concentration of Ru loading the crystallinity of the sample is steadily decreasing suggesting that the Ru particles have been doped into the crystal lattice of the TiO_2 HBNs.

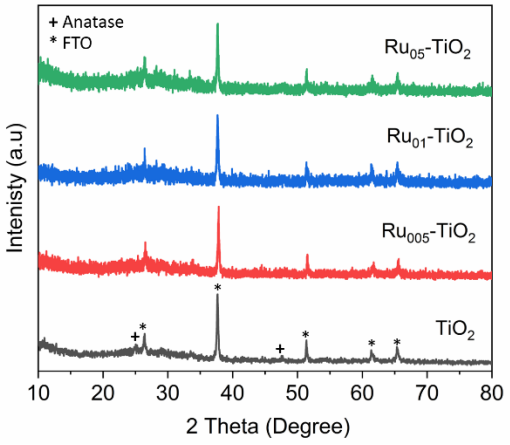

Figure 1. XRD pattern of the as prepared TiO_2 and Ru_x-TiO_2 samples.

Raman spectroscopy is more sensitive and capable of characterising the crystal structure,[38] therefore, it was used in to further investigate the crystal phases present on the TiO_2-based thin film samples. The Raman patterns of the as-prepared TiO_2 and Ru_x-TiO_2 samples are shown in Figure 2. The Raman feature of the anatase phase, positioned at 143, 395, 517, and 638 cm^{-1} are associated with the E_g, B_{1g}, A_{1g}, and E_g vibrations, respectively, was present in all the fabricated sample.[39-43] Under close inspection, the main anatase peak of sample Ru_{05}-TiO_2 positioned at 143 cm^{-1} was shifted to 149 cm^{-1}, whereas the peak positioned at 638 cm^{-1} was shifted to 621 cm^{-1}. When the

concentration of Ru was lowered down to 0.01 and 0.005 M, these shifts were reduced. These shifts are speculated to be attributed to lattice substitution of Ru into TiO_2.[44] Additionally, Raman feature of potassium titanate (PT) positioned at 285 and 444 cm^{-1}, was also observed, indicating potassium contamination from the titania precursor, PTO (Figure 2).[45] The PT and anatase peak intensities seem to have an inverse relationship, where one increases, while the other one decreases. However, a general trend can be observed, where PT peaks are found to increase in the Ru_x-TiO_2 samples. This corresponds to the loss of crystallinity observed in the XRD patterns (Figure 1) due to lattice substitution of Ti with Ru, which lowers the intensity of the anatase phase peaks No ruthenium related peak was found on the Raman spectra of the Ru_x-TiO_2 samples. This is probably due to the small particle size of RuO_2 (discussed in the next section) and low concentration, along with the low intensity Raman excitation source (785 nm).

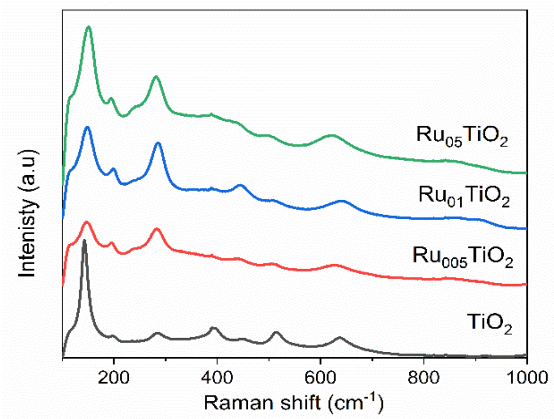

Figure 2. Raman pattern of the as-prepared TiO_2 and Ru_x-TiO_2 samples.

The morphology of the HBN structure of the titania was examined using SEM (Figure 3). The microstructured as-prepared TiO_2 was evenly coated on the FTO (Figure 3a). Each nanorod exhibited a vertically oriented spine with a highly branched nanostructure (inset of Figure 3a). When different concentration of Ru was loaded onto the TiO_2 HBN *via* solvothermal treatment, no significant alteration was observed in the Ru_x-TiO_2 samples (Figure 3b-d). However, there were noticeable nanoparticles deposited on the spine and the nano-branches of TiO_2 HBNs, which could be attributed to the agglomeration of the RuO_2 nanoparticles (inset of Figure 3b-d). The cross-section view of the as-prepared TiO_2 coating revealed the morphology of the HBNs attaching to the FTO glass (Figure 4a). The growth of nano-branches of TiO_2 HBNs was perpendicular to the FTO and was supported on a base layer of TiO_2 with 1-2 µm of thickness, which had dense and thick structures. The base layer was attached on the FTO coating on the glass. Taking a closer look at the tip of the TiO_2 nanorods, the length of the nanorod spine was measured between 1-5 µm (Figure 4b), whereas the nano-branches grown on the spine were ranged from 50-300 nm (Figure 4c). The nano-branches structure was proposed to provide high surface area exposing more active sites for the photocatalytic reaction and the loading of Ru element.[37]

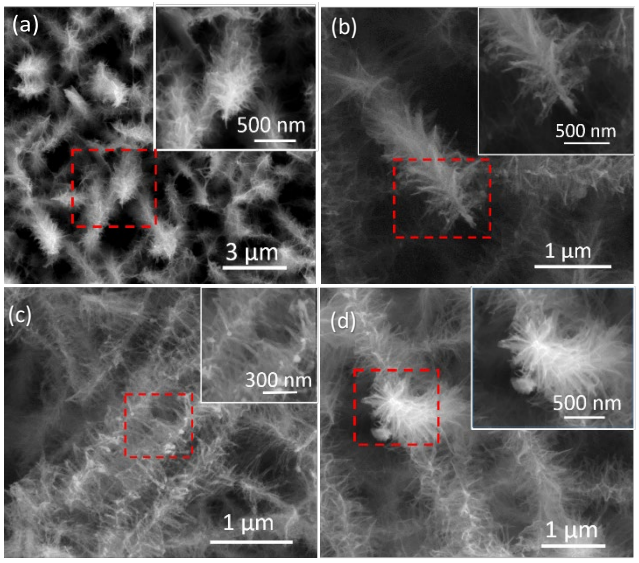

Figure 3. SEM images, with high magnification inserts indicated by the red border, of (a) as-prepared TiO_2, (b) Ru_{005}-TiO_2, (c) Ru_{01}-TiO_2, and (d) Ru_{05}-TiO_2.

The thickness of the HBN spine and nano-branches as well as the diameter of the loaded RuO_2 nanoparticles were ~60.1, 20.9, 11.2 nm, respectively (Figure 4c). The size of the loaded RuO_2 nanoparticles in Ru_{05}-TiO_2 sample was ~11.5 nm (Figure 4d). Furthermore, numerous nanoparticles of a much smaller size compared to the vicinity RuO_2 nanoparticles, were observed in the Ru_{05}-TiO_2 sample (Figure 4e). These highly dispersed nanoparticles present on the TiO_2 HBNs were ranged 1-4 nm in diameter. The EDX mapping on HR-TEM evidenced the presence of RuO_2 nanoparticles distributed along the TiO_2 HBNs.

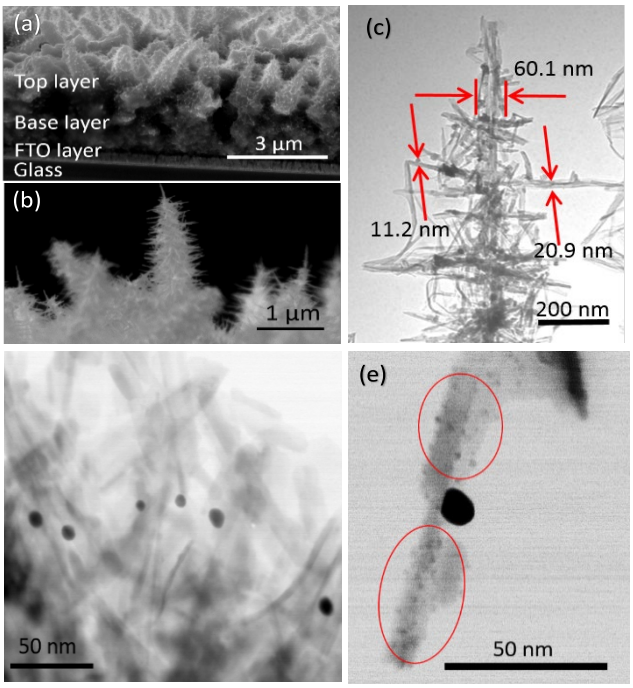

Figure 4. SEM cross-section view of the as-prepared TiO_2 sample (a, b). TEM image of a single Ru_{01}-TiO_2 HBN with thickness measurements (c). Low (d) and high (e) magnification of HR-TEM images of Ru_{05}-TiO_2 sample.

It can also be observed that Ru particles are detected in the lattice of the HBNs (Figure 5).

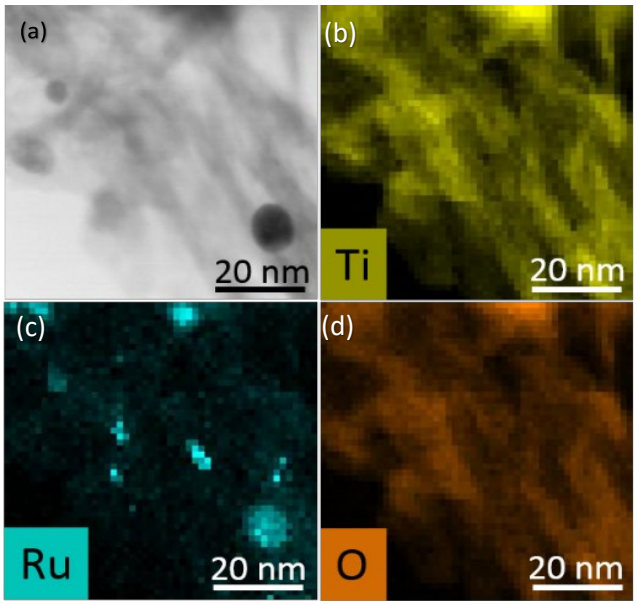

Figure 5. HR-TEM EDX mapping for Ru_{05}-TiO_2 sample.

X-ray photoelectron spectroscopy (XPS) was performed to investigate the surface properties of the fabricated TiO_2 and Ru_x-TiO_2 thin films and to estimate the amount of Ru loaded on the TiO_2 thin film (Figure 6). The Ru $3d_{5/2,}$ and $3d_{3/2}$ peaks (dark shaded area in Figure 6), which centred at 281.0 and 285.4 eV, respectively, were present in all the Ru_x-TiO_2 samples. These peaks were attributed to Ru^{4+}, indicating RuO_2 NPs were loaded onto TiO_2.[46,47] Ru^{4+} particles seem to have replaced Ti^{4+} in the HBN lattice as shown from the EDX studies (Figure 6), as well as Raman peak shifts (Figure 2) and XRD crystallisation decrease (Figure 1).The area was analysed and the concentration of Ru was estimated to be 2.82, 1.45, and 1.11 at% for the Ru_{05}-TiO_2, Ru_{01}-TiO_2, and Ru_{005}-TiO_2, respectively. As expected, no Ru peak was observed in the as-prepared TiO_2 sample. Nevertheless,

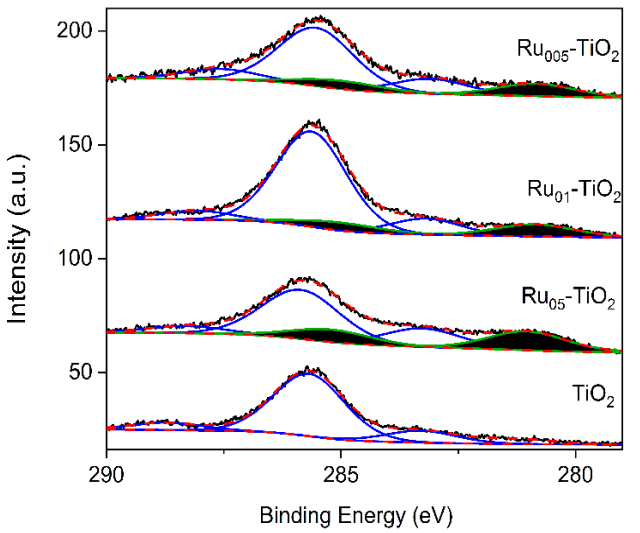

Figure 6. XPS spectra of the as-prepared TiO_2 and Ru_x-TiO_2 samples. The shaded area represented the Ru area under the curve.

The XPS spectra revealed the peak for K centred at 293.0 eV (data not shown), confirming the presence of potassium titanate in all of the thin film samples, as observed in the Raman pattern (Figure 2).[48] The C1s peaks shown centred at 283 eV, 286 eV, and 288 eV (not shaded) are ascribed to adventitious carbon contamination due to atmosphere exposure of the samples[49].

The optical properties of the synthesized thin films were investigated using UV-Vis spectroscopy. Diffuse reflectance of the as-prepared TiO_2 and Ru_x-TiO_2 samples was measured and the bandgap energy was estimated using the Kubelka-munk function (Figure 7a). The bandgap energy of the as prepared TiO_2 was ~3.6 eV, which is larger than the anatase phase of TiO_2 (~3.2 eV). The band gap widening is attributed to the quantum confinement effect of the nanostructures.[50-52] The bandgap energy for the Ru_{005}-TiO_2, Ru_{01}-TiO_2, and Ru_{05}-TiO_2, was ~3.54, 3.53 and 3.49 eV, respectively. Although the shift of the bandgap energy observed in the Ru_x-TiO_2 samples was not significant, the bandgap energy decreased with increasing Ru concentration. This phenomenon is very likely due to the Ru^{4+} present in the crystal lattice of the titania, matching the observations made earlier from EDX, XRD and in the Raman pattern of Ru_{05}-TiO_2 (Figures 1,2 and 6 respectively).[53] As confirmed by the XPS , Ru^{4+} was doped into the crystal lattice replacing Ti^{4+}, which explains the increased absorbance in the

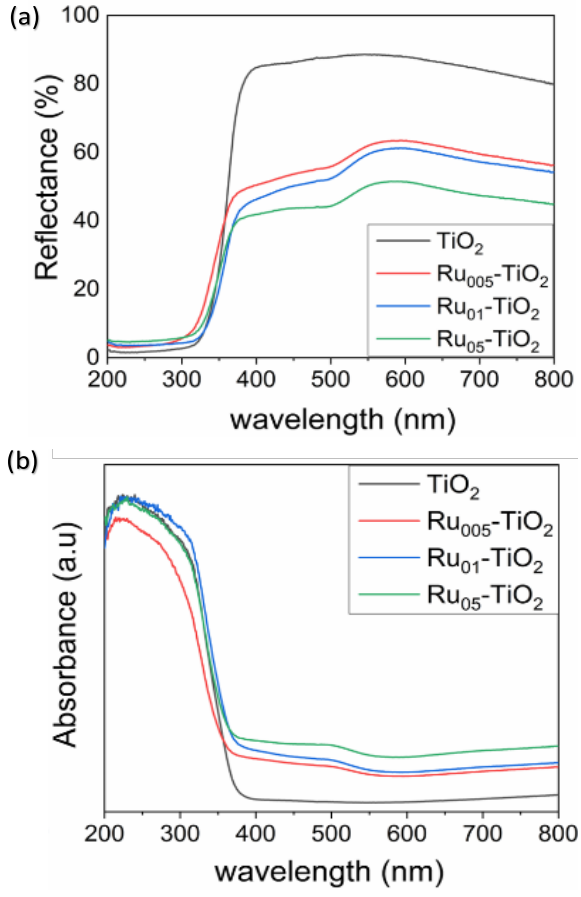

Figure 7. Diffuse reflectance (a) and absorbance (b) of the as-prepared TiO_2 and the Ru_x-TiO_2 samples.

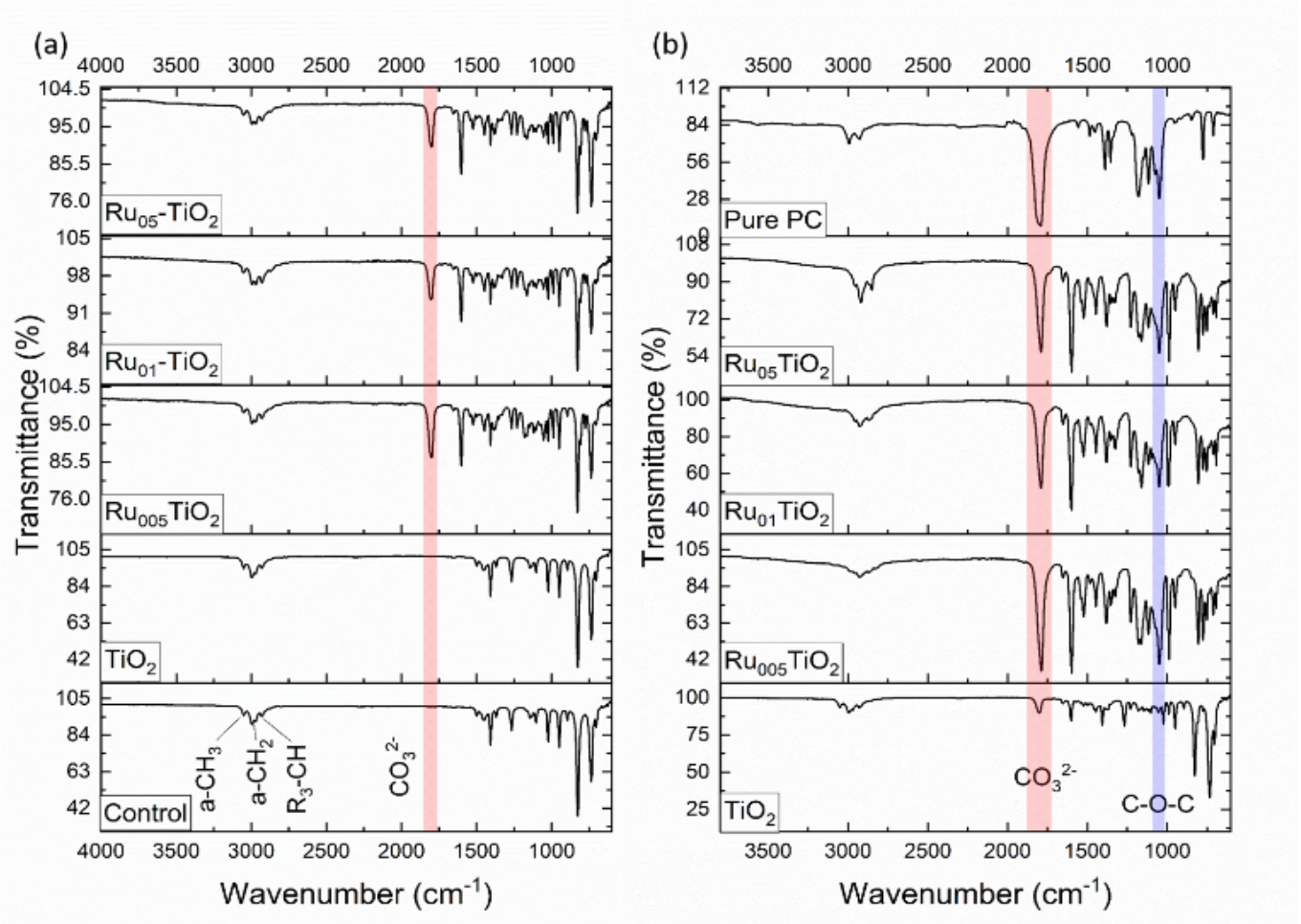

Figure 8. (a) FTIR pattern of the solution obtained before evaporation from the fabricated Ru_x-TiO_2 and the control experiment without light and photocatalyst; (b) evaporated products with the fabricated Ru_x-TiO_2 photocatalysts and pure cyclic propylene carbonate as reference.

region of 350-500 nm that is observed in Figure 7(a,b).[53-56] Another observation is that the overall absorbance increased with the Ru loading concentration. The overall increase in absorbance, for wavelengths longer than 500nm, is attributed to the RuO_2 decorated on the surface of the TiO_2 HBNs.[35] The synergistic effects of the Ru^{4+} doping and RuO_2 decoration on the TiO_2 are shown to greatly enhance the visible light absorption of the Ru_x-TiO_2 samples, making the use of a solar simulator for the photo-generation of cyclic carbonates a viable option.

Photocatalysis studies

The photocatalytic activity of the fabricated samples was evaluated with the photo-conversion of PO into PC under the irradiation of a simulated solar lamp. PC was used as a reference for CCs. A control experiment performed in the absence of photocatalyst and light was conducted. No PC was obtained as revealed in the FTIR pattern of the control experiment (Figure 8a). Only the tertiary –CH and anti-symmetry of $-CH_3$ and $–CH_2$, positioned at 2847.4, 2921.2 and 2953.1 cm^{-1}, respectively, were observed, and these were attributed to the PO moiety.[57] The as-prepared TiO_2 HBN catalyst, which was placed into the PO solution for 6 h under irradiation of the simulated solar lamp, showed no conversion. In contrast, for the fabricated Ru_x-TiO_2 photocatalyst, the trough positioned at 1792 cm^{-1} was observed, which corresponds to one of the characteristic peaks of the cyclic carbonate group.[57] The intensity of this trough increased with decreased Ru concentration. This phenomenon indicated that higher amount of PC was photo-generated with lower amount of Ru loading (Figure 8a). When the Ru loading was increased from 0.005 M to 0.01 M, the photo-generation of PC was reduced to ~50% compared to that of Ru_{005}-TiO_2 sample. Further increasing the Ru loading, however, did not reduce the photo-generation of PC significantly.

To further investigate the selectivity and purity of the photo-generation of PC, the solution was purified through evaporation to remove the DCM and unreacted PO. Then, the residue solution was analysed using FTIR (Figure 8b). The intensity of the trough, which positioned at 1792 cm^{-1}, for all the Ru_x-TiO_2 samples was enhanced in the purified solutionsThe as prepared TiO_2 HBN photocatalyst presented a weak trough at 1792 cm^{-1}, indicating small amount of CCs were produced. This confirms that the reaction is possible without the Ru doping on the TiO_2 HBNs photocatalyst; however, the doping greatly enhances its performance based on the intensity of the trough evident in Figure 8b. On the other hand, the control experiment solution when evaporated had no residual solution left, as expected. The Ru_{005}-TiO_2 sample exhibited the highest intensity among the

Ru_x-TiO_2 samples, indicating a high selectivity towards PC. Relatively to the intensity of the pure PC trough, the selectivity of each sample towards PC were estimated to be 83, 62 and 57 % for Ru_{005}-TiO_2, Ru_{01}-TiO_2, and Ru_{05}-TiO_2 samples, respectively. Moreover, another trough centred at 1048 cm^{-1}, which was assigned to another characteristic peak of the CC group (C-O-C), was present in the pure PC solution. The same trough was observed in the solution after the photocatalytic reaction with Ru_x-TiO_2 samples, confirming PC was photo-generated by the Ru_x-TiO_2 samples. An additional peak centred at 1598 cm^{-1}, which is attributed to the C=N bond, presented in all the solution after the photocatalytic reaction with Ru_x-TiO_2 samples but was absent in the pure PC solution.[58] The emergence of this peak was very likely due to the dissolution of DMAP that was used as an additive in the reacting solution.

Conclusions

TiO_2 HBN thin films have been synthesised *via* a 2-step hydrothermal method, doped with Ru^{4+} and decorated with different amount of RuO_2 nanoparticles. These novel hyper-branch microstructured TiO_2 thin films doped and loaded with Ru^{4+}/RuO_2 exhibited enhanced visible light absorption when compared to the pristine TiO_2 thin film. The size of the loaded RuO_2 nanoparticles ranged from 10 to 15 nm. The best performing amount of Ru loaded onto TiO_2 herein was 0.005 M, which was 1.11 at% Ru relative to TiO_2 as shown in the XPS analysis. The photo-generation of PC using Ru_{005}-TiO_2 sample had an estimated selectivity of 83% towards the CC. Further quantification of the selectivity measurements will be determined using gas chromatography (GC). In the absence of Ru_x-TiO_2 photocatalyst and light, no product was obtained. These novel FTO supported photocatalysts, which eliminate the need of a catalyst separation step, are the first to be reported so far. The photocatalytic approach is a newly proposed concept for the generation of CCs. Compared to the heterogeneous counterparts, which typically require temperatures up to 80-150 °C and pressure of 10-30 bar, as well as the homogeneous catalysts that currently used in industry, at 100-200 °C, and 50-100 bar, the photocatalytic approach requires temperatures up to 55 °C and 2 bar. Therefore, this approach could potentially become a significant advantage for industrial applications.

Conflicts of interest

There are no conflicts to declare.

Acknowledgements

The authors thank the financial support provided by the Engineering and Physical Sciences Research Council EP/K021796/1 and CRITICAT Centre for Doctoral Training for financial support [Ph.D. studentship to SG; Grant code: EP/L016419/1] at Heriot-Watt University. The electron microscopy facility in the School of Chemistry, University of St. Andrews, which is supported by the EPSRC Capital for Great Technologies Grant EP/L017008/1, is acknowledged.

References

1. E. Alper and O. Yuksel Orhan, *Petroleum*, 2017, **3**, 109-126.
2. M. Aresta and A. Dibenedetto, *Dalton Trans.*, 2007, DOI: 10.1039/B700658F, 2975-2992.
3. R. L. Paddock and S. T. Nguyen, *J. Am. Chem. Soc.*, 2001, **123**, 11498-11499.
4. M. North, R. Pasquale and C. Young, *Green Chemistry*, 2010, **12**, 1514-1539.
5. J. H. Clements, *Industrial & Engineering Chemistry Research*, 2003, **42**, 663-674.
6. S. Fukuoka, I. Fukawa, M. Tojo, K. Oonishi, H. Hachiya, M. Aminaka, K. Hasegawa and K. Komiya, *Catalysis Surveys from Asia*, 2010, **14**, 146-163.
7. G. Cascio, E. Manghisi, R. Porta and G. Fregnan, *Journal of medicinal chemistry*, 1985, **28**, 815-818.
8. J. W. Comerford, I. D. Ingram, M. North and X. Wu, *Green Chemistry*, 2015, **17**, 1966-1987.
9. L. Wang, P. Li, X. Jin, J. Zhang, H. He and S. Zhang, *Journal of CO2 Utilization*, 2015, **10**, 113-119.
10. J. Castro-Osma, J. Comerford, M. North and X. Wu.
11. I. G. Korosteleva, N. A. Markova, N. V. Kolesnichenko, N. N. Ezhova, S. N. Khadzhiev and N. I. Trukhmanova, *Petrol. Chem.*, 2013, **53**, 412-417.
12. H. Kawanami and Y. Ikushima, *Chemical Communications*, 2000, 2089-2090.
13. H. S. Kim, J. J. Kim, B. G. Lee, O. S. Jung, H. G. Jang and S. O. Kang, *Angewandte Chemie International Edition*, 2000, **39**, 4096-4098.
14. A. Decortes, A. M. Castilla and A. W. Kleij, *Angewandte Chemie International Edition*, 2010, **49**, 9822-9837.
15. M. North and R. Pasquale, *Angewandte Chemie*, 2009, **121**, 2990-2992.
16. X.-B. Lu, B. Liang, Y.-J. Zhang, Y.-Z. Tian, Y.-M. Wang, C.-X. Bai, H. Wang and R. Zhang, *J. Am. Chem. Soc.*, 2004, **126**, 3732-3733.
17. F. Jutz, J.-D. Grunwaldt and A. Baiker, *Journal of Molecular Catalysis A: Chemical*, 2008, **279**, 94-103.
18. J. Peng, H.-J. Yang, Y. Geng, Z. Wei, L. Wang and C.-Y. Guo, *Journal of CO2 Utilization*, 2017, **17**, 243-255.
19. V. B. Saptal and B. M. Bhanage, *Curr. Opin. Green Sustain. Chem.*, 2017, **3**, 1-10.
20. A. Zanon, S. Chaemchuen, B. Mousavi and F. Verpoort, *Journal of CO2 Utilization*, 2017, **20**, 282-291.
21. A. Buonerba, A. De Nisi, A. Grassi, S. Milione, C. Capacchione, S. Vagin and B. Rieger, *Catalysis Science & Technology*, 2015, **5**, 118-123.
22. J. Peng, H.-J. Yang, N. Song and C.-Y. Guo, *Journal of CO2 Utilization*, 2015, **9**, 16-22.
23. V. Preethi and S. Kanmani, *Materials Science in Semiconductor Processing*, 2013, **16**, 561-575.
24. G. L. Chiarello, M. V. Dozzi and E. Selli, *Journal of Energy Chemistry*, 2017, **26**, 250-258.
25. R. D. Tentu and S. Basu, *Current Opinion in Electrochemistry*, 2017, **5**, 56-62.

26. H. Ahmad, S. K. Kamarudin, L. J. Minggu and M. Kassim, *Renewable and Sustainable Energy Reviews*, 2015, **43**, 599-610.
27. D. Kong, J. Z. Y. Tan, F. Yang, J. Zeng and X. Zhang, *Applied Surface Science*, 2013, **277**, 105-110.
28. J. Z. Y. Tan, Y. Fernández, D. Liu, M. Maroto-Valer, J. Bian and X. Zhang, *Chemical Physics Letters*, 2012, **531**, 149-154.
29. J. Zhao, Y. Li, Y. Zhu, Y. Wang and C. Wang, *Applied Catalysis A: General*, 2016, **510**, 34-41.
30. J. Z. Y. Tan, N. M. Nursam, F. Xia, M.-A. Sani, W. Li, X. Wang and R. A. Caruso, *ACS Applied Materials & Interfaces*, 2017, **9**, 4540-4547.
31. P. Blanchet and V. Landry, in *Wood Composites*, ed. M. P. Ansell, Woodhead Publishing, 2015, DOI: https://doi.org/10.1016/B978-1-78242-454-3.00013-5, pp. 335-355.
32. H. Koinuma, R. Takahashi, M. Lippmaa, S.-Y. Jeong, Y. Matsumoto, T. Chikyo and S. Suzuki, in *Handbook of Advanced Ceramics (Second Edition)*, ed. S. Somiya, Academic Press, Oxford, 2013, DOI: https://doi.org/10.1016/B978-0-12-385469-8.00057-5, pp. 1103-1124.
33. J. Schneider, M. Matsuoka, M. Takeuchi, J. Zhang, Y. Horiuchi, M. Anpo and D. W. Bahnemann, *Chemical Reviews*, 2014, **114**, 9919-9986.
34. P. K. Prajapati, A. Kumar and S. L. Jain, *ACS Sustainable Chemistry & Engineering*, 2018, **6**, 7799-7809.
35. J. Tian, X. Hu, N. Wei, Y. Zhou, X. Xu, H. Cui and H. Liu, *Solar Energy Materials and Solar Cells*, 2016, **151**, 7-13.
36. F. Yoshitomi, K. Sekizawa, K. Maeda and O. Ishitani, *ACS applied materials & interfaces*, 2015, **7**, 13092-13097.
37. W.-Q. Wu, H.-S. Rao, H.-L. Feng, X.-D. Guo, C.-Y. Su and D.-B. Kuang, *Journal of Power Sources*, 2014, **260**, 6-11.
38. Y. Gong, C. Lee and C. Yang, *Journal of Applied Physics*, 1995, **77**, 5422-5425.
39. J. S. Lee, K. H. You and C. B. Park, *Advanced Materials*, 2012, **24**, 1084-1088.
40. A. León, P. Reuquen, C. Garín, R. Segura, P. Vargas, P. Zapata and P. A. Orihuela, *Applied Sciences*, 2017, **7**, 49.
41. H. C. Choi, Y. M. Jung and S. B. Kim, *Vibrational Spectroscopy*, 2005, **37**, 33-38.
42. T. Ohsaka, *Journal of the Physical Society of Japan*, 1980, **48**, 1661-1668.
43. Y. Zhang, C. X. Harris, P. Wallenmeyer, J. Murowchick and X. Chen, *The Journal of Physical Chemistry C*, 2013, **117**, 24015-24022.
44. W.-K. Jo, S. Kumar, M. A. Isaacs, A. F. Lee and S. Karthikeyan, *Applied Catalysis B: Environmental*, 2017, **201**, 159-168.
45. X. Liu and N. Coville, *A Raman Study of Titanate Nanotubes*, 2005.
46. X. Wei, Q. An, Q. Wei, M. Yan, X. Wang, Q. Li, P. Zhang, B. Wang and L. Mai, *Phys. Chem. Chem. Phys.*, 2014, **16**, 18680-18685.
47. S. Kaliaguine, in *Stud. Surf. Sci. Catal.*, Elsevier, 1996, vol. 102, pp. 191-230.
48. Q. Wang, Z. Guo and J. S. Chung, *Mater. Res. Bull.*, 2009, **44**, 1973-1977.
49. M. Descostes, F. Mercier, C. Beaucaire, P. Zuddas and P. Trocellier, *Nuclear Instruments and Methods in Physics Research Section B: Beam Interactions with Materials and Atoms*, 2001, **181**, 603-609.
50. E. Roduner, *Chemical Society Reviews*, 2006, **35**, 583-592.
51. M. A. Siddiqui, V. S. Chandel and A. Azam, *Appl. Surf. Sci.*, 2012, **258**, 7354-7358.
52. T. Takagahara and K. Takeda, *Phys. Rev. B*, 1992, **46**, 15578-15581.
53. T.-D. Nguyen-Phan, S. Luo, D. Vovchok, J. Llorca, S. Sallis, S. Kattel, W. Xu, L. F. Piper, D. E. Polyansky and S. D. Senanayake, *Physical Chemistry Chemical Physics*, 2016, **18**, 15972-15979.
54. T. Ohno, F. Tanigawa, K. Fujihara, S. Izumi and M. Matsumura, *Journal of Photochemistry and Photobiology A: Chemistry*, 1999, **127**, 107-110.
55. H. Huang, J. Lin, G. Zhu, Y. Weng, X. Wang, X. Fu and J. Long, *Angewandte Chemie International Edition*, 2016, **55**, 8314-8318.
56. M. T. Uddin, Y. Nicolas, C. Olivier, T. Toupance, M. M. Müller, H.-J. Kleebe, K. Rachut, J. Ziegler, A. Klein and W. Jaegermann, *The Journal of Physical Chemistry C*, 2013, **117**, 22098-22110.
57. L. Zhang, X. Luo, Y. Qin and Y. Li, *RSC Adv.*, 2017, **7**, 37-46.
58. V. Kuryanov, M. K Tokarev, T. A Chupakhina, V. Ya and Chirva, *The Synthesis of N-Acetylglucosamine Heteroaromatic N-β-Glycosides under Phase Transfer Conditions: Part III. l,2,4-Triazolin-3-one Glucosaminides*, 2011.